Resonant Electron Capture and Stripping in Moderately Large-Angle Atomic Collisions*

F. P. ZIEMBA,† G. J. LOCKWOOD, G. H. MORGAN, AND E. EVERHART
Physics Department, University of Connecticut, Storrs, Connecticut

(Received January 21, 1960)

Differential scattering of ions by atoms in the energy range of 1 kev to 200 kev has been studied. The incident ion, after a single collision which is hard enough to result in a 5° deflection, was analyzed to determine whether it had captured or lost electrons. The angle 5° was chosen as a typical moderately large angle and held fixed as the energy of the incident ion was varied. When the electron capture probability is plotted vs energy, one or more peaks are observed. For the symmetrical case of He^+ on He, seven peaks are clearly outlined. Four peaks appear in the H^+ on He combination and three with H^+ on H_2. Single or double peaks are found in other cases studied which include H^+ on N_2, O_2, air, Ne, Ar, and Kr; H_2^+ on H_2 and He; H_3^+ on H_2 and He; He^+ on H_2, Ne, Ar, and Kr; N^+ on Ar; N_2^+ on N_2; Ne^+ on Ne and Ar; Ne^{++} on Ne and Ar; Ar^+ on Ar; and Kr^+ on Kr. For each case the probabilities for electron capture, scattering without change of charge, and various degrees of electron stripping are plotted vs energy. In those cases in which the electron capture probability curve has more than two peaks, these peaks are nearly evenly spaced when the probabilities are plotted vs the time of the interaction. This indicates an electron exchange effect whose period is of the order of 10^{-16} second. In cases where there are many electrons involved in the colliding atoms the phenomenon is more complicated, but vestiges of this resonant exchange are sometimes observed.

1. INTRODUCTION

A RECENT letter by Ziemba and Everhart[1] demonstrated a rather striking behavior in large-angle collisions of He^+ on He. The incident ion, after undergoing a single collision which is hard enough to result in a 5° deflection, was analyzed to determine whether it had captured or lost electrons. The electron capture probability plotted vs incident ion energy shows seven pronounced peaks. A subsequent paper by Ziemba and Russek[2] attributed this effect to the resonant process $He^+ + He \rightleftarrows He + He^+$. These results led to the present study in which many other ion-atom combinations were examined to determine whether they exhibit similar phenomena. The angle 5° was arbitrarily chosen as being representative of a typical large-angle scattering. It is large enough to insure deep interpenetration of the colliding atoms during the collision. For light ion-atom collisions the data are not sensitive to the choice of this angle.

A theoretical discussion of electron capture phenomena, including references to earlier papers, will be found in a recent paper by Bates and Lynn.[3] Total electron capture cross-section data frequently referred to in the present paper will be found in a compilation by Allison.[4] Differential measurements of ion-atom collisions which form a background for this work include those of Fedorenko[5] and Kaminker and Fedorenko.[6] More directly, the present work is a continuation of an experimental program described in papers by Carbone et al.,[7] Fuls et al.,[8] and Jones et al.[9] Generally, these papers[5–9] have studied, at fixed incident ion energy, the angular distribution and states of ionization of particles scattered in single collisions between relatively heavy ions and atoms. The present work has included many lighter ion-atom combinations and has measured instead the energy dependence of various processes at fixed scattering angle.

A description of the apparatus and experimental procedure is given in Sec. 2. Section 3 presents an impulse approximation calculation for the distance of closest approach in ion-atom collisions. This forms a basis for the discussion of the data. Section 4 presents and discusses the data for each collision combination in turn.

2. APPARATUS AND PROCEDURE

The University of Connecticut heavy-ion accelerator was used in this work. This Cockcroft-Walton accelerator can furnish magnetically analyzed beams of ions in an energy range extending from 1 kev to 200 kev. Some details of the collision chamber and the associated detection system are shown in Fig. 1 which is a modification of the apparatus used and described previously.[7–9]

a. Collision Chamber

The collision chamber and detector are inside a large box connected to the accelerator vacuum system which

* This work was supported by the Office of Ordnance Research, U. S. Army, through the Boston Ordnance District and Watertown Arsenal Laboratories.

† Now at Hughes Aircraft Company, Culver City, California.

[1] F. P. Ziemba and E. Everhart, Phys. Rev. Letters **2**, 299 (1959).

[2] F. P. Ziemba and A. Russek, Phys. Rev. **115**, 922 (1959).

[3] D. R. Bates and N. Lynn, Proc. Roy. Soc. (London) **253**, 141 (1959).

[4] S. K. Allison, Revs. Modern Phys. **30**, 1137 (1958).

[5] N. V. Fedorenko, J. Tech. Phys. (U.S.S.R.) **24**, 784 (1954).

[6] D. M. Kaminker and N. V. Fedorenko, J. Tech. Phys. (U.S.S.R.) **25**, 2239 (1955).

[7] R. J. Carbone, E. N. Fuls, and E. Everhart, Phys. Rev. **102**, 1524 (1956).

[8] E. N. Fuls, P. R. Jones, F. P. Ziemba, and E. Everhart, Phys. Rev. **107**, 704 (1957).

[9] P. R. Jones, F. P. Ziemba, H. A. Moses, and E. Everhart, Phys. Rev. **113**, 182 (1959).

maintains an operating pressure of about 5×10^{-6} mm of Hg. The collision chamber consists of two parts bridged by a flexible bellows. The first part is rigidly fixed. It contains the hole *a* which defines the incoming ion beam and the removable Faraday cage (shown in dotted outline) which measures the ion beam within the collision chamber. The flexible bellows allows the second part to rotate through any angle of scattering up to 40° about the center of the effective target volume located at point *b*. The second part contains the resolution holes *c* and *d*; it also supports the electrostatic analyzer and the detector. The detector rotates independently about a virtual axis located at *f*. The scattering geometry is nearly the same as that shown in Fig. 2 of reference 8.

A target gas pressure within the collision chamber of about one micron of mercury is maintained by differential pumping through holes *a* and *c*. This is low enough to ensure that almost all of the detected particles result from single collisions, as shown by a linear dependence of the scattered particle current on pressure. The ion beam ranged from about 10^{-7} ampere at 100 kev to 10^{-9} ampere at 1 kev. (The focusing properties of the accelerator are best at the higher energies.)

Collisions which happen to occur near *b* and which result in a scattering in the proper direction allow particles to pass through the resolution holes *c* and *d*. The electrostatic analyzer following hole *d* separates the scattered particles according to their charge state before they enter the detector. The scattered particle current was usually a few hundred particles per second; the extreme range was from 10^5 particles per second to a few particles per second.

b. Detection System

A ten-stage Dumont type 6467 electron multiplier was used as the detector. The photosensitive surface and glass envelope were removed, the ions being allowed to strike the first dynode directly. The output pulses were amplified and electronically counted.

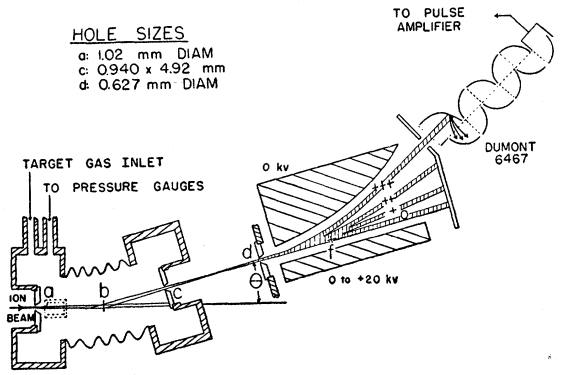

FIG. 1. The collision chamber and the associated detection apparatus.

It was found that exposure of the dynode structure to air for even a few minutes resulted in a decrease in the average pulse height by nearly a factor of 100 thereby rendering the detector inadequate. To avoid this loss of gain it was necessary to remove the envelope and install the multiplier while under an atmosphere of dry nitrogen. The sensitivity of a particular multiplier was also observed to decrease slowly, the useful lifetime being approximately two months. The data were reproducible with different multipliers.

c. Procedure

The total scattered particle current was measured by setting the detector along the axis defined by *b*, *c*, and *d*, with zero voltage on the analyzer. The neutral component was measured by applying a positive voltage to the lower analyzer plate, sweeping out the charged particles. The charged components were determined by positioning the detector as shown in the figure. The several charged components were successively deflected to the detector by applying different voltages to the analyzer. The fractions P_0, P_1, P_2, $\cdots$ were determined, where P_0 is the ratio of the neutral particle current to the total particle current, P_1 is the ratio of the current of singly-ionized particles to the total particle current, P_2 is the ratio of the current of doubly-ionized particles to the total particle current, etc.

As an illustration of the experimental procedure, consider a typical determination of P_0 at a given energy. With the detector in position to receive the total particle current or the neutral component as described above, the electronic counter was automatically run through the following cycle: (1) accumulate counts for five seconds, (2) hold for recording (during this holding time the ion beam was also measured), and (3) erase. The analyzer voltage was alternately turned on and off until ten readings of the total scattered particle current and ten readings of the neutral component were obtained along with the twenty recordings of the ion beam. The target gas supply was then cut off and the above procedure repeated to determine the scattering due to the presence of residual gas target atoms in the collision chamber. The correction for residuals was subtracted after normalization. This correction was significant only for collisions involving light ions incident upon light target atoms such as H^+ on He and reached fifty percent in extreme cases. These data were averaged to determine the fraction P_0.

d. Properties of the Detector

Although a knowledge of the absolute counting efficiency of the detector is not necessary for a determination of the fractions P_n, it has been assumed that the relative counting efficiency is independent of the charge, i.e., neutral atoms are counted as efficiently as (say) triply charged ions of the same atom with the

same velocity. It was not possible to make a direct calibration of counting efficiency vs charge state, but there are a number of indirect indications that the above assumption is reasonable:

(1) Fuls[8] and Jones[9] measured a beam of ions with both an electron multiplier and a Faraday cage. Their measurements at 25 to 100 kev showed that the current gain of the multiplier was independent of the charge state of the ion ranging from singly to quadruply charged particles. One would not expect neutral particles to be different.

(2) Absolute differential scattering cross sections[8,9] for He^+ on He collisions taken at 25 to 100 kev are in excellent agreement with the Rutherford formula, making the assumption that the current gain is independent of the charge state.

(3) A single-channel pulse-height analyzer was used in the present work to determine the differential pulse-height distribution in a number of typical cases. The distribution is found to be the same for neutrals, singly-ionized, doubly-ionized, etc., particles. This indicates that the number of secondary electrons emitted from the first dynode per incident particle is independent of the charge state, i.e., the relative counting efficiencies are the same.

(4) There are theoretical reasons[2] for believing that the He^+ on He data should oscillate about the fifty percent line. The experimental data of Fig. 4(a) show this nearly to be the case. If there were a difference in counting efficiency for neutrals and singly-charged particles, the level of the P_0 curve would be shifted up or down accordingly. The agreement suggests that the relative counting efficiencies of He^0 and He^+ are nearly the same.

Finally, it should be noted that any differences in the relative counting efficiencies would affect the peak heights but would not cause a significant shift in their locations.

Although there was considerable evidence that the detector was charge independent, it is noticeably energy dependent below about 10 kev. Since it was not possible to calibrate the detector vs energy, an extension of the data below 10 kev required that the first dynode be held at ground potential so that neutral atoms and charged particles arrived with the same velocity. In our preliminary measurements[1] of the He^+ on He combination the first dynode had been held at -2500 volts, the He^+ ions thereby receiving a post-acceleration not experienced by the He^0 particles. This resulted in a more efficient detection of the charged particles and a gradual falloff of the P_0 curve below 10 kev. The data below 10 kev reported in the present work was obtained with the first dynode at ground potential. Most of the data above 10 kev was obtained with the dynode at -2500 volts, but representative cases showed that the data above 10 kev did not depend on the arrangement within the experimental error. The small changes in location of the peaks in the P_0 curve for He^+ on He of Fig. 4(a) as opposed to Fig. 1 of reference 1 are due to a voltage recalibration.

3. CONCERNING LARGE-ANGLE COLLISIONS

a. Classical Orbits

It has been shown both theoretically[10] and experimentally[8] that large-angle scattering of ions by atoms at kilovolt energies can be described in terms of classical orbits. A Coulomb potential modified by exponential screening is used:

$$V(r)=(Z_1Z_2e^2/r)\exp(-r/a). \tag{1}$$

Here, Z_1e and Z_2e are the nuclear charges of the colliding atoms and a is a screening length. Often a is taken to be equal to $a_0/(Z_1^{\frac{2}{3}}+Z_2^{\frac{2}{3}})^{\frac{1}{2}}$ where $a_0=0.53\times10^{-8}$ cm. There is a useful relation between the angle of scattering $\theta_{c.m.}$ in center-of-mass coordinates and the distance of closest approach r_0. This relation[11] is

$$\theta_{c.m.}a/b=K_1(r_0/a), \tag{2}$$

where K_1 is a modified Bessel function of the second kind of order unity, and b is defined by

$$b=Z_1Z_2e^2/E_{c.m.}, \tag{3}$$

where $E_{c.m.}=$ the initial kinetic energy in the center-of-mass system. The energy in center-of-mass and laboratory systems depends on the mass ratio γ according[12] to $E_{c.m.}=E_{lab}/(1+\gamma)$. and the corresponding angles (in the small angle case) are given by $\theta_{lab}=\theta_{c.m.}/(1+\gamma)$. Using the above relationships and Eq. (2), one can readily calculate r_0 as a function of θ_{lab}, E_{lab}, Z_1, and Z_2.

Figure 2(a) plots r_0/a_0 vs incident ion energy E_{lab} in kev for several ion-atom combinations with $\theta_{lab}=5°$. It is readily seen that for combinations of light gases such as H^+ on He, the incident proton nearly passes through the center of the target He atom at all energies. This is shown schematically in Fig. 2(b) where paths of the incident proton are shown at 1-, 10-, and 100-kev energies. The solid circle has a radius a_0 while the dotted circle has a radius equal to the target atom, namely the radius of maximum radial charge density for He. For fixed incident ion energy it should be noted that rather large changes in the angle of scattering would correspond to very small changes in r_0 on an atomic scale. These results will be useful for interpreting the data to be presented.

Figure 2(b) also depicts the combinations H^+ on Ne and Ne^+ on Ne. In the latter case the distance of closest approach is large on an atomic scale at even

[10] E. Everhart, G. Stone, and R. J. Carbone, Phys. Rev. **99**, 1287 (1955).

[11] This analytic solution to Eq. (18) of reference 10 was pointed out by John L. Carter, Jr. in a private communication.

[12] See for example, L. I. Schiff, *Quantum Mechanics* (McGraw-Hill Book Company, Inc., New York, 1949), Sec. 18.

the highest energies. One should also expect a considerable variation in r_0 as the angle of scattering is varied at fixed energy. This result provides a basis for a qualitative understanding of the heavy ion-atom collisions. Combinations such as H^+ on Ne are intermediate.

b. Use of Protons and Deuterons

Since they are electronically equivalent, protons (p) and deuterons (d) were in certain cases used alternatively as incident projectiles on the same target atom. An elementary calculation shows that the condition for equal relative velocities is

$$E_{\text{lab}}{}^d=(m_d/m_p)E_{\text{lab}}{}^p=2E_{\text{lab}}{}^p, \tag{4}$$

while the simultaneous condition for equal distances of closest approach to a target atom of arbitrary mass is found to be

$$\theta_{\text{lab}}{}^d=(m_p/m_d)\theta_{\text{lab}}{}^p=(\tfrac{1}{2})\theta_{\text{lab}}{}^p. \tag{5}$$

For example, the collision of (say) a 5 kev (lab) proton with (say) a helium atom which results in a scattering with $\theta_{\text{lab}}=5°$ is equivalent to a 10 kev (lab) deuteron scattering on helium with $\theta_{\text{lab}}=2.5°$. An experimental advantage was obtained by using deuterons rather than protons at low energies. Since the accelerator was designed to operate at rather high energies, the ion beam was both defocused and unstable below 5 kilovolts. Using a deuteron beam, the accelerator voltage was twice that of the equivalent proton beam

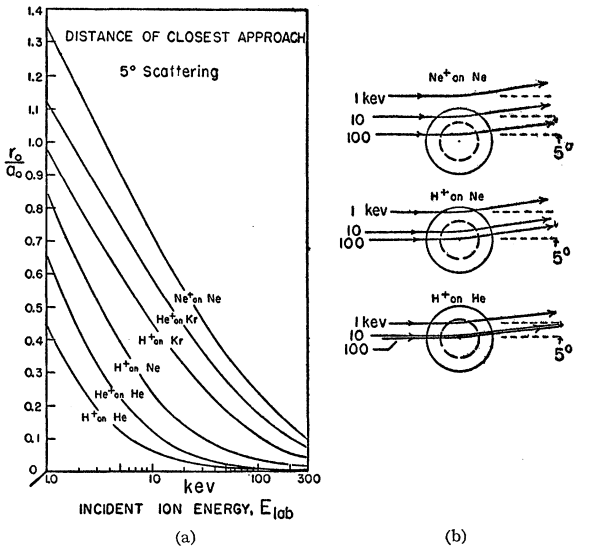

FIG. 2. (a) The distance of closest approach r_0 in units of the Bohr radius a_0 is plotted vs the incident ion energy E_{lab} in kev for several ion-atom combinations. The angle of scattering $\theta_{\text{lab}}=5°$ for all cases. (b) Paths of the incident ion at 1, 10, and 100 kev are shown schematically for three representative combinations. The solid circle has a radius a_0. The dotted circle has a radius equal to that of the target atom.

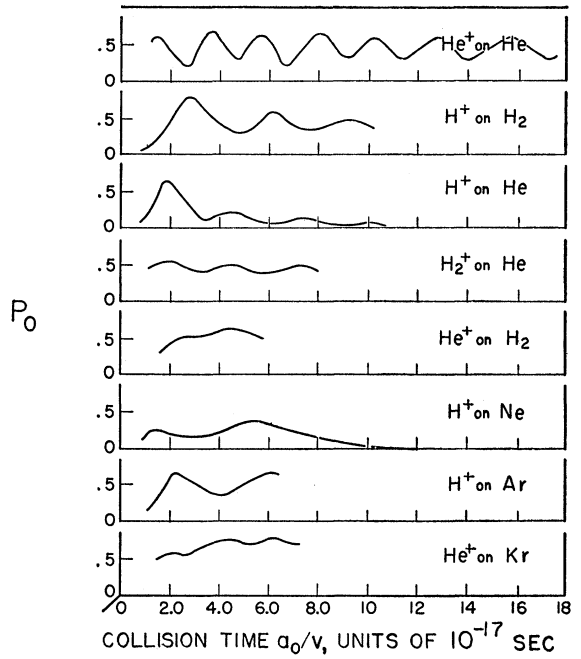

FIG. 3. The electron capture (or exchange) probability vs collision time. The fraction P_0 is plotted vs collision time a_0/v for several of the combinations which show resonant electron capture. Here v is the relative velocity and the interaction length is arbitrarily taken to be the Bohr radius a_0.

and hence more stable. In practice, the data could be carried to lower energies with the equipment available.

The data for D^+ on He was erronously taken at $\theta_{\text{lab}}=3°$ rather than the preferred $\theta_{\text{lab}}=2.5°$. However, the charge analysis is insentitive to the scattering angle. This was pointed out earlier and can be seen by the agreement between the H^+ on He and D^+ on He data of Fig. 4(c) in the energy region where the data overlap.

4. DATA AND DISCUSSION

The data are presented in Figs. 4–9. Except for Fig. 9, the fractions P_n of the scattered current in each charge state are plotted vs incident ion energy at a fixed angle of scattering (usually 5°). These fractions P_0, P_1, P_2, P_3, $\cdots$ correspond respectively to electron exchange (or capture), scattering without a change in charge, single electron stripping, double stripping, etc. In cases where only three charge states are possible, the values for P_1, are not shown for the sake of clarity but are readily found since P_0, P_1, and P_2 must add to unity. Figure 3 plots P_0 vs collision time a_0/v for several of the combinations which demonstrate resonant electron capture. Here v is the relative velocity and the interaction length is arbitrarily taken to be the Bohr radius a_0. Of course the effective interaction length is different for each of the ion-atom combinations, and therefore Fig. 3 can be used only for semiquantitative comparisons.

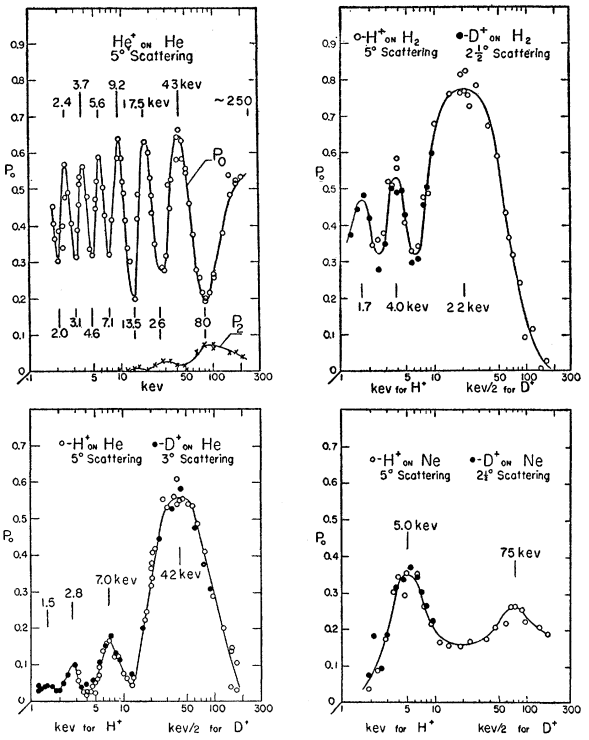

FIG. 4. The electron capture (or exchange) probability vs incident ion energy for single collisions of He^+ on He, H^+ on H_2, H^+ on He, and H^+ on Ne. The fraction P_0 of the particles scattered through an angle $\theta_{lab}=5°$ which capture an electron during the collision is plotted vs the incident ion energy E_{lab} in kev. The data are extended to low energies in several cases by using deuterons as described in the text.

a. He^+ on He

Figure 4(a) shows the experimental results for the He^+ on He combination. Preliminary measurements on this combination were reported by the authors in a letter.[1] The modification of the detector which is described in Sec. 2d above resulted in a substantial improvement of the low-energy data over that reported previously.

Scattered particles from this collision have also been analyzed to determine their charge state in two earlier papers,[8,9] the data being taken as a function of the scattering angle at fixed energy as opposed to the procedure followed in the present work. The significant result obtained was there was hardly any variation to the charge-state fractions of the scattered helium particle as the scattering angle was varied from 1° to 20°. These results are to be found in Fig. 4 of reference 8 and Fig. 2 of reference 9. The present results for 5° scattering show maxima in the curve for P_0 at 2.4, 3.7, 5.6, 9.2, 17.5, and 43 kev, and indications of a maximum at about 250 kev. Figure 3 shows that these peaks are nearly evenly spaced in collision time. The curve for P_2 shows peaks at 13.5, 26, and 80 kev and is zero at lower energies. Peaks for P_2 occur where P_0 is a minimum.

A theoretical discussion of this case based upon the impact parameter method has been given in another paper.[2] The nuclei are assumed to move in classically describable orbits and quantum theory is applied to determine the probability of electron exchange as a function of the impact parameter and relative velocity. Since the nuclear charges are equal, the ground-state eigenfunction of the quasi-molecule formed during the collision must be described by a linear combination of symmetric and antisymmetric eigenfunctions. For the case of exchange without excitation, the coefficients in this linear combination are constant during the collision, but the relative phase, which depends upon the difference in eigen-energies of the symmetric and antisymmetric states, is altered by the collision. This phase change corresponds to an electron being transferred periodically from one nucleus to the other during the collision. Both the velocity (energy) and impact parameter (scattering angle) variations of the calculated exchange probability are in qualitative agreement with the experimental results. A discussion of exchange with excitation is included.

b. H^+ on H_2

Figure 4(b) presents the results for H^+ on H_2 suitably extended to lower energies by the inclusion of D^+ on H_2 data (as discussed in Sec. 3b above). The P_0 curve shows peaks at 1.7, 4.0, and 22 kev. When these data are plotted vs collision time as in Fig. 3, the above peaks appear to be the first three in a series which are nearly equally spaced in collision time. There appears to be two alternative interpretations of these data:

(1) The total electron capture cross section[4] for H^+ on H_2 exhibits a maximum at about 8 kev and a maximum of this sort is characteristic of nonsymmetrical ion-atom collisions. This suggests that the incident proton be regarded as interacting with the target hydrogen molecule as a whole in so far as electronic states are concerned. The data thus reflect an oscillation between two eigenfunctions of a quasi-molecule, one corresponding to the electron being in the neighborhood of the incident proton, the other corresponding to the electron being associated with the target H_2 molecule. This oscillation occurs throughout the collision with a period of about 10^{-16} seconds.

(2) The similarity between the H^+ on H_2 and He^+ on He data, however, suggests an alternative possibility. The two atoms of the target H_2 molecule are very far apart compared to the distance of closest approach for a 5° scattering at kilovolt energies (see Fig. 2). Therefore the incident proton passes very close to only one member of the molecule, and the interaction might possibly be regarded as H^+ on H. It might be mentioned in this respect that total electron capture cross section calculations for the collision H^+ on H have often been compared to experimental measurements of H^+ on H_2.

An experimental study of the H^+ on H reaction is currently under way at this laboratory.

c. H^+ on He

Figure 4(c) shows the results for H^+ on He, again extended to lower energies with D^+ on He data. Peaks for P_0 occur at 1.5, 2.8, 7.0, and 42 kev. Although this collision is not of the symmetrical type, Fig. 3 shows that these four peaks appear to be the first four in a series which are nearly equally spaced in collision time. In this nonsymmetrical collision the successive peaks of P_0 become lower at lower energies, in contrast to the symmetrical He^+ on He case where the successive peaks are of about the same height. In spite of the rather large energy defect, the behavior of P_0 is strikingly like that discussed by Bates and Lynn[3] for electron capture of the accidental resonance type. Figure 1 of that paper may be compared with our Fig. 4(c). It should be noted that different scales are used in these two figures. Detailed calculations are necessary before a direct comparison can be made. A direct experimental study of the inverse reaction He^+ on H is under way at this laboratory. The total electron capture cross section[4] exhibits a single maximum at about 25 kev for H^+ on He.

d. H^+ on Ne

Figure 4(d) gives the results obtained for H^+ on Ne. The data are anomalous in comparison with those obtained for protons on the other noble gases. The curve for P_0 shows two widely separated peaks at 5.0 and 75 kev. The high-energy peak is rather small and P_0 does not drop off rapidly at high energies as does the data for H^+ on He, Ar, and Kr. There is no evidence of any additional peaks below the one at 5.0 kev. The behavior at low energies might be attributed to the rapid increase of r_0 at low energies shown in Fig. 2. Figure 3 shows the data plotted vs collision time. The total electron capture cross section[4] exhibits a peak at about 10 kev.

e. H^+ on Ar

Figure 5(a) shows the data for H^+ on Ar. The P_0 curve shows a peak at 30 kev. Qualitative data for energies less than 10 kev (unpublished) suggest another peak at about 4 kev.

f. H^+ on Kr

Figure 5(b) which gives the data for H^+ on Kr is similar to that obtained for H^+ on Ar. The P_0 curve shows a peak at 30 kev. Qualitative data for energies below 10 kev (unpublished) suggest another peak at about 3 kev. An examination of Fig. 2 shows that the incident proton does not penetrate deeply into the target Kr atom. The data at low energies is expected to have some angular dependence for this collision.

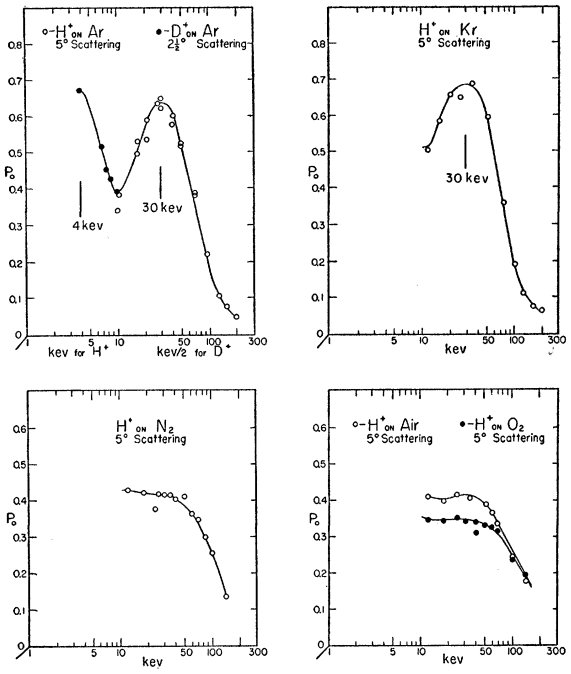

FIG. 5. The electron capture probability vs incident ion energy for single collisions of H^+ on Ar, H^+ on Kr, H^+ on N_2, H^+ on air, and H^+ on O_2. The fraction P_0 of particles scattered through an angle $\theta_{lab}=5°$ which capture an electron during the collision is plotted vs the incident ion energy E_{lab} in kev. The data for H^+ on Ar are extended to low energies by using deuterons as described in the test.

g. H^+ on N_2

Figure 5(c) shows the results obtained for H^+ on N_2. This collision as well as H^+ on O_2 is important in upper atmospheric phenomena. The P_0 curve exhibits a change of slope near 40 kev. Unpublished data below 10 kev suggests a broad peak in P_0 at about 4 kev for H^+ on N_2, O_2, and dry air.

h. H^+ on O_2 and Air

Figure 5(d) shows that the data for H^+ on dry air is nearly identical with that obtained for H^+ on N_2 as expected. The data for H^+ on O_2 is also shown.

i. H_2^+ on He

Figure 6(a) shows the results for H_2^+ on He. The P_0 curve exhibits maxima at 5.0, 14, and 75 kev. Over the entire energy region investigated, the charged component of the scattered particle current was found to be in the form H^+. No H_2^+ scattered ions were ever detected. Although the detection apparatus cannot distinguish between H^0 and H_2^0, the absence of H_2^+ ions indicated that the incident ion dissociated during the collision. If the dissociation were to take place early in the collision one might regard half of the collisions to be of the form H^+ on He the other half H^0 on He. Although no data is available for the latter, H^+ on He

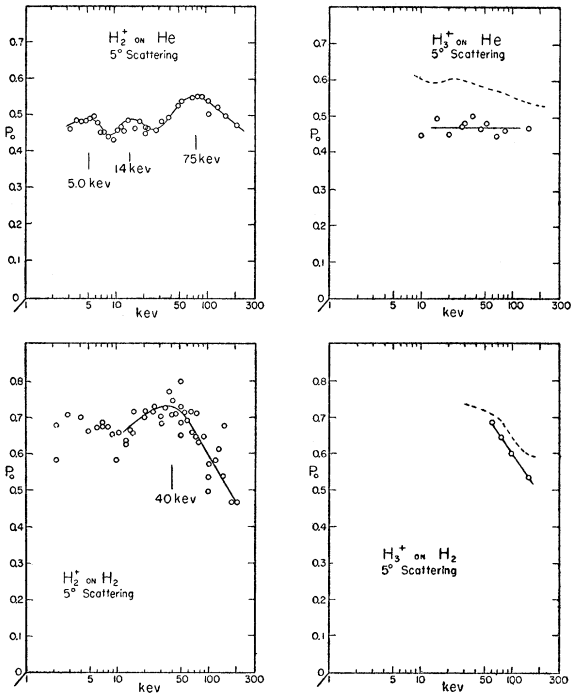

FIG. 6. The electron capture probability vs incident ion energy for single collisions of H_2^+ on He, H_3^+ on He, H_2^+ on H_2, and H_3^+ on H_2. The fraction P_0 of particles scattered through an angle $\theta_{lab}=5°$ which capture an electron during the collision is plotted vs the incident ion energy E_{lab} in kev. The dotted curves are the predictions of the simple breakup model described in the text.

has been investigated and discussed earlier [Fig. 4(c) and Sec. 4(c)]. Any increase in P_0 above 0.5 must be attributed to the process H^+ on $He \rightarrow H+He^+$ according to this simple model. A comparison of Figs. 6(a) and (4c) shows that the peaks in P_0 occur at the same relative velocity (not energy) as expected. This result may also be seen in Fig. 3. A combination of the H^+ on He and H_2^+ on He data using the assumption above, can be used to estimate the behavior of the H^0 on He collision. This estimate along with the data of H^+ on He may in turn be used to predict the results to be expected for the collision H_3^+ on He. Thus P_0 for H_3^+ is supposed to be the average of those for two H^0 and one H^+ on the same target. The dotted curve of Fig. 6(b) demonstrates this prediction. The agreement is rather poor and suggests that the above simple model is not valid. It is emphasized that the data are to be compared at equal relative velocities, not equal laboratory energies. This combination H_2^+ on He is compared with the inverse combination He^+ on H_2 in Sec. 4(m) below.

j. H_3^+ on He

Figure 6(b) presents the H_3^+ on He data. There is considerably more scatter in these data than other combinations studied due to the small H_3^+ ion beam produced by the accelerator. The dotted curve shows the prediction of the simple model described in Sec. 4i above. It is to be noted that all of the scattered charged particles appeared as H^+. The absence of H_2^+ and H_3^+ scattered ions indicated that the incident ion dissociated during the collision.

k. H_2^+ on H_2

Figure 6(c) gives the results for H_2^+ on H_2. Although this would appear to be a case of symmetrical resonance, rather like He^+ on He electronically, multiple peaks were not found. The curve for P_0 shows a broad peak at about 40 kev. The H_2^+ ion was found to dissociate during the collision and this may explain the difference. This combination was the only one where we experienced difficulty in obtaining reproducible data. The scatter in the data may be hiding fine structure. It is to be noted that the highest energy peaks for H_2^+ on H_2 and H^+ on H_2 [Figs. 6(c) and 4(b)] occur at the same relative velocity as is required by the simple model described in Sec. 4i. Following the argument described previously in Sec. 4i, these data may be used to predict the results for the H_3^+ on H_2 collision. This prediction is shown as a dotted curve in Fig. 6(d). The agreement is inconclusive in this case.

l. H_3^+ on H_2

Figure 6(d) presents data for H_3^+ on H_2 as well as the prediction based upon the simple model described in Secs. 4i and 4k. No H_2^+ or H_3^+ scattered ions were

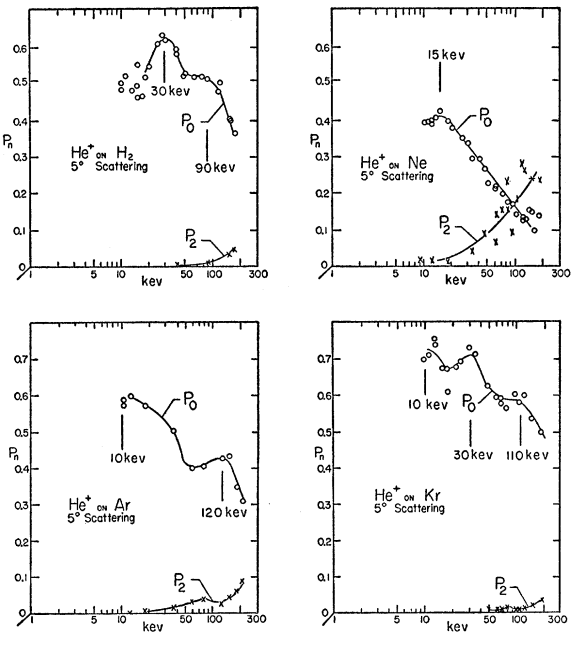

FIG. 7. The electron capture probability vs incident ion energy for single collisions of He^+ on H_2, He^+ on Ne, He^+ on Ar, and He^+ on Kr. The fraction P_0 of particles scattered through an angle $\theta_{lab}=5°$ which capture an electron during the collision is plotted vs the incident ion energy E_{lab} in kev. The fraction P_2 is also shown.

detected, indicating a complete dissociation of the incident H_3^+ ion during collision.

m. He^+ on H_2

Figure 7(a) shows the data for the He^+ on H_2 collision which is the inverse of the H_2^+ on He collision of Sec. 4i above. Considerable excitation is suggested by the rapid increase in P_2 above 50 kev. The P_0 curve exhibits a peak at 30 kev and an inflection at about 90 kev. These data are plotted vs collision time in Fig. 3 where they may be most easily compared with the results obtained for H_2^+ on He and H^+ on He.

n. He^+ on Ne

Figure 7(b) presents the results for He^+ on Ne which show a peak at 15 kev. The values for P_1 are not shown but are readily found since P_0, P_1, and P_2 must add to unity. Figure 5 of reference 8 and Fig. 3 of reference 9 presents data for P_n vs θ_{lab} at 25, 50, and 100 kev; these data show clearly that the fractions P_n are insensitive to a change in the angle of scattering θ_{lab}.

o. He^+ on Ar

Figure 7(c) shows the data for He^+ on Ar. The P_0 curve exhibits broad maxima at about 10 and 120 kev. Some qualitative data (unpublished) taken below 10 kev suggest another minor peak at about 7 kev. The data for P_2 is also shown in the figure. Results for P_n vs θ_{lab} at 25, 50, and 100 kev are to be found in Fig. 6 of reference 8 and Fig. 4 of reference 9.

p. He^+ on Kr

Figure 7(d) presents the data for He^+ on Kr. The value of P_0 exhibits peaks at 10 and 30 kev and an inflection at 110 kev. Two additional peaks at about 2 and 7 kev are suggested by (unpublished) qualitative data taken below 10 kev. The data for P_2 are also shown in the figure.

q. Ne^+ on Ne

Figure 8(a) presents the data for Ne^+ on Ne. The angular variation of the fractions P_n at 25, 50, and 100 kev are shown in Fig. 7 of reference 8 and Fig. 5 of reference 9. It is to be emphasized that in references 8 and 9, the fractions P_n were determined vs scattering angle θ_{lab} at fixed energy; in the present work, the fractions P_n were determined vs incident ion energy E_{lab} at fixed scattering angle $\theta_{lab}=5°$. All of these data show that the degree of electron stripping increases with increasing energy, corresponding to decreasing distances of closest approach r_0. The several stripping probabilities each in turn reach a maximum at higher energies as the number of electrons lost increases.

Since this collision is symmetrical, a behavior similar to that exhibited by He^+ on He was expected. Although

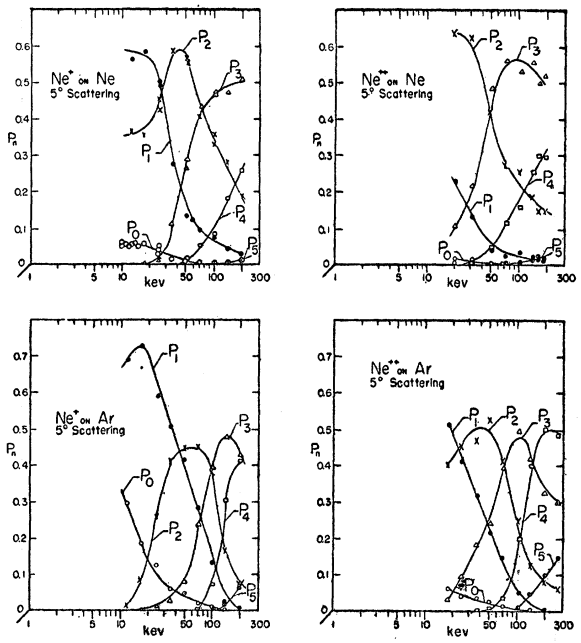

FIG. 8. The charge analysis vs incident ion energy for single collisions of Ne^+ on Ne, Ne^{++} on Ne, Ne^+ on Ar, and Ne^{++} on Ar. The fractions P_n are plotted vs the incident ion energy E_{lab} in kev at fixed scattering angle $\theta_{lab}=5°$.

there is no evidence of an oscillatory behavior in the P_0 curve of Fig. 8(a), resonant exchange effects were observed when P_0 was measured vs θ_{lab} at several fixed energies. These results are shown in Fig. 10(a) and discussed in Sec. 4y.

r. Ne^{++} on Ne

Figure 8(b) gives the results for Ne^{++} on Ne. The presence of a P_0 fraction indicates that double electron capture has occurred in a single collision. In this case particularly, a plot was made of Ne^0 particle current vs target gas pressure (similar to that shown in Fig. 3 of reference 7). The linearity of the plot demonstrated that this is, indeed, a single collision phenomenon.

s. Ne^+ on Ar

Figure 8(c) presents the data for Ne^+ on Ar. The angular variation of the fractions P_n at 25, 50, and 100 kev are shown in Fig. 8 of reference 8 and Fig. 6 of reference 9. Qualitative data below 10 kev (unpublished) indicate a peak in P_0 at about 6 kev.

t. Ne^{++} on Ar

Figure 8(d) shows the results obtained for Ne^{++} on Ar. Double electron capture is also (see Sec. 4r) observed in this combination.

u. Ar^+ on Ar

Figure 9(a) presents the data for Ar^+ on Ar. The angular variation of the fractions P_n at 25, 50, and 100

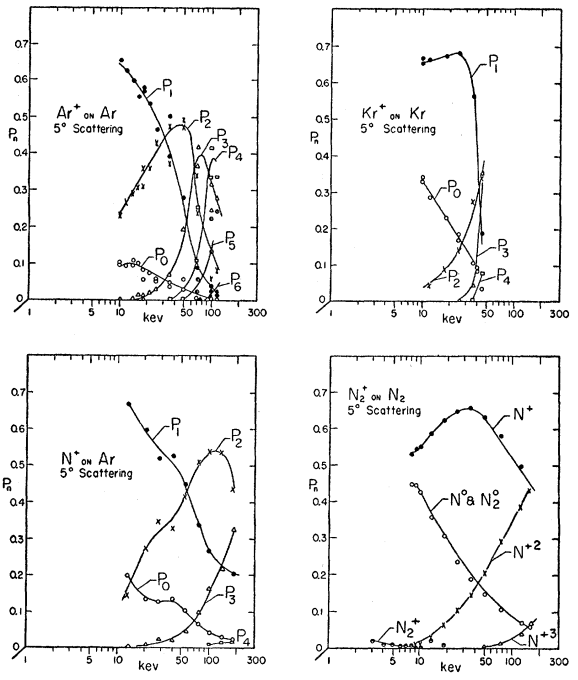

FIG. 9. The charge analysis vs incident ion energy for single collisions of Ar^+ on Ar, Kr^+ on Kr, N^+ on Ar, and N_2^+ on N_2. The fractions P_n are plotted vs the incident ion energy E_{lab} in kev at fixed scattering angle $\theta_{lab}=5°$.

kev are shown in Fig. 9 of reference 8 and Fig. 7 of reference 9. The curve for P_0 shows a peak at 12 kev and qualitative data below 10 kev (unpublished) indicate another peak at about 3 kev. Resonant exchange effects are observed when P_0 is measured vs θ_{lab} at several fixed energies. These results are shown in Fig. 10(b) and discussed in Sec. 4z. A theoretical discussion of the Ar^+ on Ar collision has been given in two papers by Russek and Thomas.[13,14]

v. Kr^+ on Kr

Figure 9(b) shows the results obtained for Kr^+ on Kr. The data could not be extended to high energies due to limitations of the magnetic ion beam analyzer. The angular variation is shown in Fig. 10(c) and discussed in Sec. 4aa.

w. N^+ on Ar

Figure 9(c) presents the results obtained for N^+ on Ar. The data show that multiple electron stripping of nitrogen is significantly less probable than for the noble gases Ne, Ar, and Kr at comparable energies. The contrast is also apparent when one compares the angular variation of the fractions P_n for N^+ on Ar with (say) Ne^+ on Ar. Figure 10(d) plots P_n vs θ_{lab} for 100 kev N^+ on Ar. The data for Ne^+ on Ar shown in Fig. 8 of reference 8 show considerably more angular dependence.

x. N_2^+ on N_2

Figure 9(d) shows the data for N_2^+ on N_2. At energies less than 20 kev, a small fraction of the ions are found to be scattered as N_2^+ without dissociating. Since the collision is symmetrical, one could expect resonance effects to be observable at low energies; none are observed above 10 kev. The curve for P_0 must be regarded as the sum $N_2^0+N^0$. Qualitative data below 10 kev (unpublished) show a peak in P_0 at about 7 kev.

y. Ne^+ on Ne, Angle Varied

Figure 10(a) presents data for P_0 vs θ_{lab} at 10 and 15 kev with Ne^+ on Ne. These data demonstrate an oscillatory behavior. [See also Fig. 8(a) and Sec. 4q]. As discussed in Sec. 4a, the exchange probability P_0 is in general a function of the impact parameter (or r_0 or θ_{lab}) and relative velocity (or energy). On the basis of the results obtained for the He^+ on He collision discussed in reference 2, one would expect an oscillation of P_0 vs θ_{lab} for collisions in which $r_0/a_0>0.1$. Since excitation and ionization are more important in the

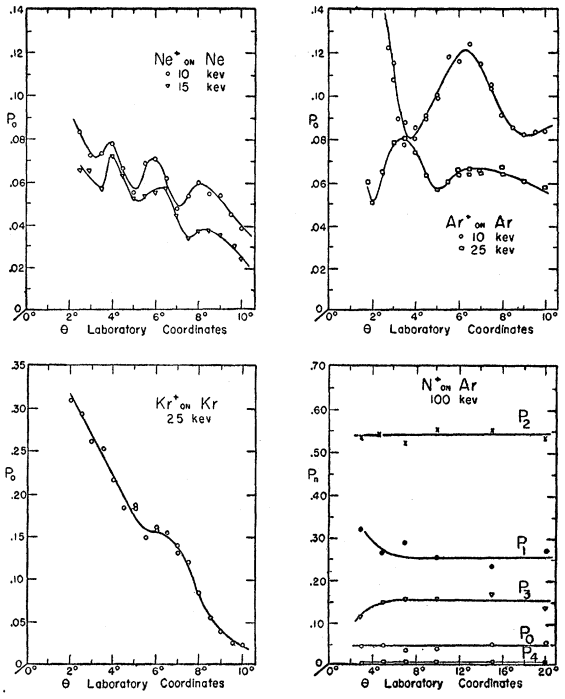

FIG. 10 The electron exchange probability vs scattering angle for single collisions of Ne^+ on Ne, Ar^+ on Ar, and Kr^+ on Kr. The fraction P_0 of particles which capture an electron during the collision is plotted vs the laboratory scattering angle θ at several fixed incident ion energies. The charge analysis for 100-kev N^+ on Ar is plotted vs the laboratory scattering angle.

[13] A. Russek and M. T. Thomas, Phys. Rev. **109**, 2015 (1958).
[14] A. Russek and M. T. Thomas, Phys. Rev. **114**, 1538 (1959).

heavier ion-atom collisions, P_0 is expected to decrease with increasing energy and scattering angle.

z. Ar^+ on Ar, Angle Varied

Figure 10(b) shows the data for P_0 vs θ_{lab} at 10 and 25 kev with Ar^+ on Ar. The results are similar to those obtained for Ne^+ on Ne described above.

aa. Kr^+ on Kr, Angle Varied

Figure 10(c) presents data for P_0 vs θ_{lab} at 25 kev with Kr^+ on Kr. The results are similar to those obtained for Ne^+ on Ne and Ar^+ on Ar.

bb. N^+ on A, Angle Varied

Figure 10(d) presents data for P_n vs θ_{lab} at 100 kev with N^+ on A. The fractions P_n are seen to be nearly independent of θ_{lab}, unlike the results obtained for other heavy ion-atom collisions studied in references 8 and 9.

5. ACKNOWLEDGMENTS

We wish to thank Dr. A. Russek for many valuable discussions of the data, Dr. P. R. Jones for helpful advice in the earlier phases of this work, and Mr. Seymour Kessler for his assistance in taking the data.

PHYSICAL REVIEW VOLUME 118, NUMBER 6 JUNE 15, 1960

Experimental Verification of the "Incoherent Scattering" Theory for the Transport of Resonance Radiation

A. V. PHELPS AND A. O. MCCOUBREY*
Westinghouse Research Laboratories, Pittsburgh, Pennsylvania
(Received January 20, 1960)

The predictions of the incoherent scattering theory of the transport of resonance radiation developed by Holstein and by Biberman are shown to agree with laboratory measurements of the decay constants for the intensity of the mercury 2537 A resonance radiation following a period of optical excitation. Also, the relative importance of the diffusion of resonance atoms and the escape of resonance radiation as mechanisms for the destruction of mercury atoms in the $^3P_1$ or resonance state are determined from measurements of decay constants as a function of mercury density and cell radius. The experimental results show that diffusion of the resonance atoms is negligible and that the predictions of imprisonment theory are confirmed to within 15%. The experiment sets an upper limit to the diffusion coefficient at unit gas density for atoms in the $^3P_1$ state of 5×10^{17} cm^{-1} sec^{-1} at 340°K, which is consistent with a value of 4×10^{16} cm^{-1} sec^{-1} predicted using the frequency of excitation transfer collisions calculated by Holstein. The success of the theories based on completely incoherent scattering of resonance radiation points to the desirability of including this feature in the treatment of those astrophysical problems in which the spectral line shape is determined by Doppler broadening or by collision broadening.

I. INTRODUCTION

A NUMBER of theories have been developed to describe the transport of resonance radiation through the parent gas. When this process involves a large number of successive absorption and reemission events, the predictions of the theories are found to vary considerably with the assumed relation between the frequency of the absorbed photon and the frequency of the reemitted photon. In most treatments of radiative transfer[1] it is assumed that the frequency of the absorbed and re-emitted photons are identical, i.e., the scattering is "coherent" with regard to frequency (although not necessarily so with regard to phase). These theories have been used to predict the rate of escape of resonance radiation in laboratory experiments,[1] e.g., the decay of intensity of the mercury 2537 A line following a period of optical excitation. The predicted decay constants for radiation at the center of the resonance line are two orders of magnitude too small to explain experimental observations at the higher gas densities. This fact led to the use of an average absorption coefficient or "equivalent opacity" for the resonance radiation[2] in

* Now at the National Company, Incorporated, Melrose, Massachusetts.

[1] S. Chandrasekhar, *Radiative Transfer* (Oxford University Press, New York, 1950). See especially Sec. 90. See also R. v.d. R. Woolley and D. W. N. Stibbs, *The Outer Layers of a Star* (Oxford University Press, New York, 1953), Chap. VIII. For a recent discussion of coherence in scattering at low densities see J. P. Barrat, J. Phys. radium **20**, 541, 633, and 657 (1959).

[2] A discussion of early efforts to bring the theory into agreement with experiment are given in reference 3 and A. G. C. Mitchell and M. W. Zemansky, *Resonance Radiation and Excited Atoms* (The Macmillan Company, New York, 1934), pp. 230–236. The values of g obtained using Milne's formula for the decay constant of the central portion of the resonance line vary from 0.63 to 0.012 times those in reference 11 as k_0L increases from 2 to 400. The values of g obtained using Sampson's equivalent opacity in Milne's formula for the decay constant for the intensity of resonance radiation vary from 1.1 to 28 times those given in reference 11 as k_0L changes from 2 to 400. Finally, the g values obtained by Zemansky from Kenty's size dependent diffusion coefficients (reference 18) are about 20% below the values given in reference 11 and are in very good agreement with the values obtained by Holstein.[3]